Viktoriya Boyko, Thomas Link, Kostiantyn Mykhalenkov

Structure characterization and precipitation in two Al-Mg-Si-Mn casting alloys

Charakterystyka struktury oraz procesy wydzieleniowe w dwóch stopach odlewniczych układu Al-Mg-Si-Mn

Abstract

The as-cast structure of permanent mould (PM) (alloy l) and high-pressure die castings (HPDC) (alloy 2) of the AlMg5Si2Mn alloy has been investigated by differential scanning calorimetry, microhardness measurements, transmission electron microscopy, and energy dispersive X-ray analysis. Inside the α-Al grains in both alloys, curved plate-like precipitates were detected in both alloys. Examination of these precipitates revealed a number of features, such as: (1) the composition of the precipitates is very close to the stochiometric Mg_2Si compound; (2) precipitates are aligned along dislocations; (3) the precipitate density is much higher for high-pressure die castings where the α-Al matrix contains more dislocations than in permanent mould castings; (4) precipitates lie inside the α-Al grains where they are randomly distributed. Between the Mg_2Si larnellas, precipitates were not observed. Microhardness tests show that the hardness of the alloy cast into a permanent mould is lower than that of a high-pressure die casting. This observation reveals the origin of high strength in an AlMg5Si2Mn alloy subjected to HPDC.

Keywords: aluminium casting alloy, precipitates, element distribution, natural hardening

Streszczenie

Przy wykorzystaniu różnicowej kalorymetrii skaningowej, pomiarów mikrotwardości, elektronowej mikroskopii transmisyjnej oraz mikroanalizy rentgenowskiej zbadano mikrostrukturę stopu AlMg5Si2Mn, odlewanego kokilowo (stop 1) oraz wysokociśnieniowo (stop 2), w stanie wytworzenia (po odlaniu). W obydwu stopach wewnątrz ziaren α-Al roztworu stałego obserwowano zakrzywione wydzielenia płytkowe. Badanie tych wydzieleń pozwoliło na określenie szeregu ich cech, takich jak: (1) stechiometryczne podobieństwo składu chemicznego ze związkiem Mg_2Si; (2) ustawienie wydzieleń wzdłuż linii dyslokacji; (3) większa gęstość wydzieleń w przypadku

Viktoriya Boyko Ph.D. student, **Thomas Link Associated Professor**, **Doctor:** Technical University Berlin, Germany; **Kostiantyn Mykhalenkov Professor, Doctor:** National Technical University of Ukraine, Kiev Polytechnic Institute, Ukraine; mykhalenkov@yandex.ua

odlewów wysokociśnieniowych, w których osnowa α-Al roztworu stałego zawiera więcej dyslo-kacji niż w przypadku odlewu kokilowego; (4) losowe rozmieszczenie wydzieleń w obrębie α-Al roztworu stałego. Pomiędzy płytkami Mg_2Si wydzielenia nie występują. Pomiary mikrotwardości pokazały, że twardość stopu odlewanego do kokili jest mniejsza niż odlewanego pod wysokim ciśnieniem, wyjaśniając tym samym przyczynę wysokiej wytrzymałości stopu AlMg5Si2Mn odle-wanego wysokociśnieniowo.

Słowa kluczowe: odlewniczy stop aluminium, wydzielenia, element rozkładu, utwardzanie na-turalne

1. Introduction

Designing new lightweight alloys for continuous replacement of iron and steel parts is now mainstream in energy saving and the improvement of fuel efficiency in the trans-portation sector. In parallel to the powerful advances of aluminum wrought alloys, the search for novel efficient casting alloys still attract attention of both researchers and manufacturers of aluminum casting. The last few decades have shown a growing interest in Al-Mg-Si-Mn casting alloys, considered potential competitors for current well-estab-lished materials. Despite the active implementation of Al-Mg-Si-Mn alloys into foundry practice, there has been a lack of research performed over structure formation and, es-pecially, their "natural hardening".

The commercial attraction of Al-Si cast alloys is mainly attributed to the discovery of the modified Al-Si eutectic made by Dr. Aladar Pacz in around 1920 [1, 2]. He found that that the brittle (Al) + (Si) eutectic changed its morphology from undesired long plates (see Fig. 1a) to fine acicular fibers when small amounts of alkali fluoride, sodium, or po-tassium were added to the melt. Since the potential of changing the morphology of Si plates growing in the course of eutectic solidification to fibers by modification was estab-lished, the popularity of Al-Si alloys began.
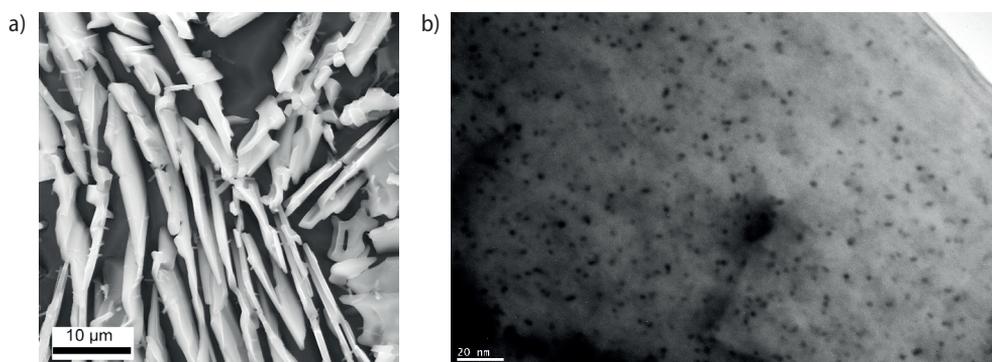

Fig. 1. Morphology of Si in (Al)-(Si) eutectic in non-modified A356 commercial casting alloy (a) (deep etching) and bright field image of precipitates of β" phase in A356 after T6 heat treatment (b)

Following the accidental discovery of age hardening in Al-Cu-Mg alloys made by Alfred Wilm [3, 4], it was proposed to add to Al-Si alloys 0.2–0.5 wt.% Mg to make them age-hardenable [5, 6]. It has been found that the yield strength of Al-Si-Mg alloys in a T6 condition are more than double that of binary Al-Si alloys containing the same quantity of Si. Figure 1b represents the bright field image of precipitates of β'' phase formed in an A356 alloy artificially aged at 175°C for 6 hours.

After these advances, casting alloys of the Al-Si system have been the most widespread materials in foundry shops to this day, and the A356 alloy containing 7 wt.% Si and 0.3 wt.% Mg is known as the "working horse" for the aluminum casting industry.

Recently, another group of casting alloys has gained its renaissance. Being long in the shadow of commercial Al-Si-Mg alloys, Al-Mg-Si-Mn casting alloys returned to the market in 1996 [7–9]. It was reported by Wuth et al. [7] that an alloy with a nominal composition of AlMg5Si2Mn possessed high ductility (up to 18%), yield strength (up to 220 MPa), and ultimate tensile strength (up to 350 MPa) when subjected to high-pressure die casting. Simultaneously, these alloys displayed several advantages in comparison to established commercial Al-Si casting alloys.

Comparing AlSi7Mg and AlMg5Si2Mn casting alloys, the most intriguing is that the highest strength for AlSi7Mg is only achieved after heat treatment, but AlMg5Si2Mn exhibits the highest prosperities in the as-cast state.

In this article, the as-cast state of the AlMg5Si2Mn alloy after permanent mould (PM) casting and high-pressure die casting (HPDC) is considered, and the characterization of the structure, element distribution, and precipitates present in the as-cast state in the AlMg5Si2Mn alloy are given in a broad scale.

2. Experimental

Two Al-Mg-Si-Mn–type alloys were the subjects of our research program. Their chemical composition is represented in Table 1.

Table 1. Chemical composition of alloys under investigation

Specimen	Elements content, wt.% (Al – balance)							
	Mg	Si	Mn	Cu	Zn	Ti	Be	Fe
1	5.32	2.12	0.58	0.001	0.001	0.02	–	0.03
2	5.47	2.20	0.69	0.02	0.01	0.1	0.004	0.12
3	0.32	6.97	0.02	–	–	0.01	–	0.06

The first one (specimen 1) was prepared using a resistant furnace and graphite crucible (batch weight of 0.25 kg). The starting materials were Al (99.9% purity), Mg (99.9% purity), as well as AlSi25 and AlMn26 master alloys. Before casting, the melt was treated

by blowing for 10 min. After blowing, the surface of the melt was skimmed to remove dross and cast into a permanent mould (PM). The casting temperature was 710°C and the mould temperature 22°C. This condition gives a cooling rate of 5 K·s^{-1} (see Fig. 2a). The second one (specimen 2) was supplied by "Aluminium Rheinfelden GmbH" in the form of a 3-mm-thick high-pressure die casting plate (HPDC) (see Fig. 2b).

Fig. 2. Macrostructure of permanent mould cast ingot (specimen 1) (a) and high pressure die casting (specimen 2) (b)

Differential scanning calorimetry (DSC) measurements were performed using a NETZSCH DSC 404 instrument. During DSC measurements, specimens were protected under an argon atmosphere with a flow rate of 75 ml min^{-1}. The measurements were performed from 20 to 700°C at heating rate 10°C·min^{-1}.

Heating experiments for a commercial A356 (AlSi7Mg) casting alloy was also included in the research program for comparison of eutectic melting temperatures (specimen 3) as well as precipitation behavior.

Samples for microstructure observations were cut from ingots, mounted into Technovit resin, and ground and polished using conventional metallographic techniques. The microstructures were recorded using a light microscope fitted with a digital camera and utilizing image-capture software.

Transmission electron microscopy observations were carried out on thin foils cut from bulk samples. Disks with a 3 mm diameter and 150 μm thickness were electrolytic polished in a twin-jet STRUERS Tenupol 3 electrolytically thinning apparatus in a solution containing 70% methanol, 20% glycerol, and 10% perchloric acid held at −27°C under 20 V voltages. Specimens were examined with a Philips TM-30 microscope operated at 300 kV accelerating voltage and equipped with the Thermo Scientific EDS system. Element distribution was measured using a spot size of 4–8 nm.

3. Experimental results

3.1. Differential scanning calorimetry

In a DSC experiment, the specimen under investigation and a reference specimen are heated up respectively and cooled down simultaneously. The reference specimen must not show any phase transition within the investigated temperature range. The difference in energy consumption or production per time and mass between specimen and reference is measured during such a heating cycle. This so-called heat flow is plotted as a function of temperature. A positive peak indicates an exothermic reaction, namely a solidification or precipitation. A negative peak stands for an endothermic reaction; i.e., melting or dissolution.

DSC plots obtained from the as-cast specimens during heating are shown in Figure 3. In specimen 3, three peaks can be distinguished, denoted as heat effect 1, 2, and 3. Their characteristic temperatures at start ('peak onset'), extreme ('peak'), and end ('peak offset') are summarized in Table 2.
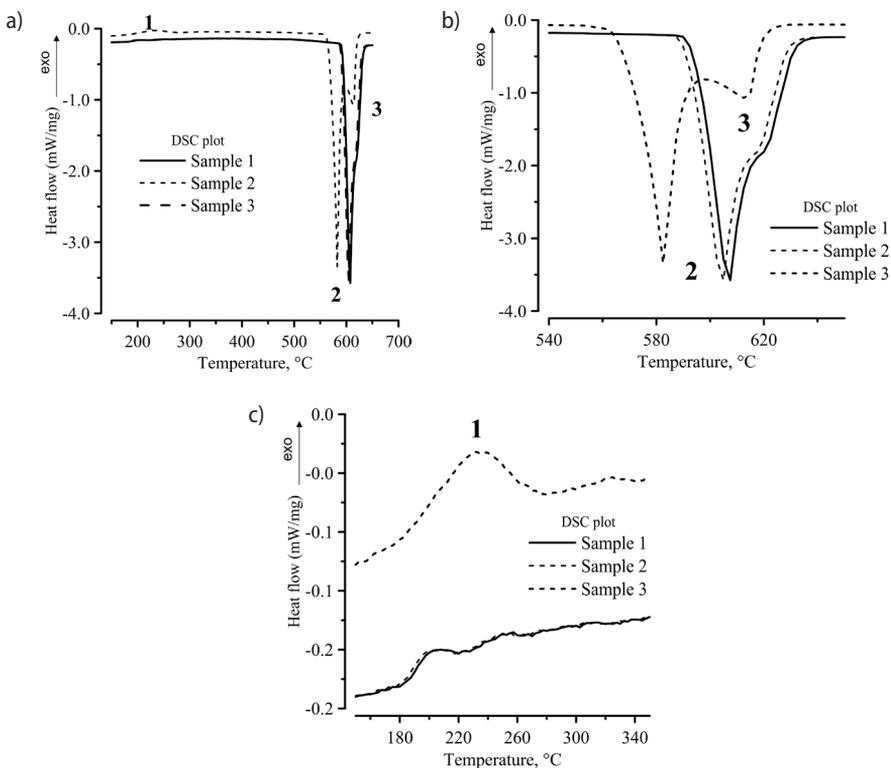

Fig. 3. DSC traces for specimens 1, 2 and 3 at a heating rate 10 K·s⁻¹: a) DSC plot over the full temperature range; heat effects marked as 1, 2, 3; b) spread endothermic heat effects 2 and 3; c) spread exothermic heat effect 1, visible only in sample 3

Table 2. Characteristic temperatures of heat effects observed during heating of samples 1 and 3

Peak	Sample 1	Sample 3
Heat effect 1, °C (exothermic)		
Peak onset	–	220.0
Peak	–	247.8
Peak outset	–	262.1
Heat effect 2, °C (endothermic)		
Peak onset	596.2	574.4
Peak	609.0	591.0
Peak outset	618.0	608.7
Heat effect 3, °C (endothermic)		
Peak onset	618.0	608.7
Peak	624.3	619.1
Peak outset	632.4	625.1

Specimen 2 shows the same strong peaks (2 and 3) as specimen 1, but not the small peak (1). This first thermal reaction during heating is an exothermic effect with peak onset at 220.0°C and peak temperature of 247.8°C detected only in specimen 3. The next thermal reaction was observed at a peak onset temperature of 596.2°C for specimen 1 and 574.4°C for specimen 3.

This endothermic effect is attributed to the melting of (Al) + (Mg_2Si) and (Al) + (Si) eutectics, subsequently. Further heating resulted in the appearance of an endothermic peak with onset 618.0°C for specimens 1 and 2, and 608.7°C for specimen 3. This effect is related to the melting of α-Al (Fig. 3b).

According to the established results on the precipitation behavior of wrought Al-Mg-Si alloys (6001, 6111, etc.), the temperature range of observed thermal effect 1 correlated with precipitation of β'' phase [10, 11]. It has been found by [10] exothermic effect at 207–308°C is associated with β'' precipitation. TEM and DSC examinations performed by M. Vedani [11] showed the β''/β' needle-shaped precipitates aligned along the $\langle 100 \rangle_{Al}$ direction and can be identified in the aged matrix structures.

For cast alloys, there are few works that have been published. Considering as-cast age hardening AlSi7Mg casting alloys, the authors [12] detected exothermic peak in the temperature range 180–260°C – similar to the behavior of sample 3 (see Fig. 3c). They associated this thermal effect with precipitation of the needle-shaped coherent β'' phase.

For specimens 1 and 2, thermal events that can be associated with the precipitation process in an as-cast state were not distinctly identified.

3.2. Microstructure observations

In this section, the microstructural features are presented at increasing magnification starting at the scale of the microstructure. Figure 4 represents the polished microstructure of specimens 1 and 2.

The microstructure of both samples consists of primary α-Al grains (appear light) and (Al) + (Mg$_2$Si) eutectic (appear grey), consistent with the established Al-Mg-Si phase diagram [10] where the alloys with Mg/Si ration in the range 2.4–3.0 are positioned inside the two-phase area. Specimen 1 exhibits dendritic morphology of α-Al grains surrounded by eutectic colonies. For specimen 2 equiaxed, globular-rosette morphology is preferential. The average grain size in specimen 2 is about 20–40 µm and cannot be compared to specimen 1, where the average length of primary dendrite arms was greater than 250 µm and varies from columnar crystals in the area close to the mould wall to large equiaxed grains in the central part of the casting.
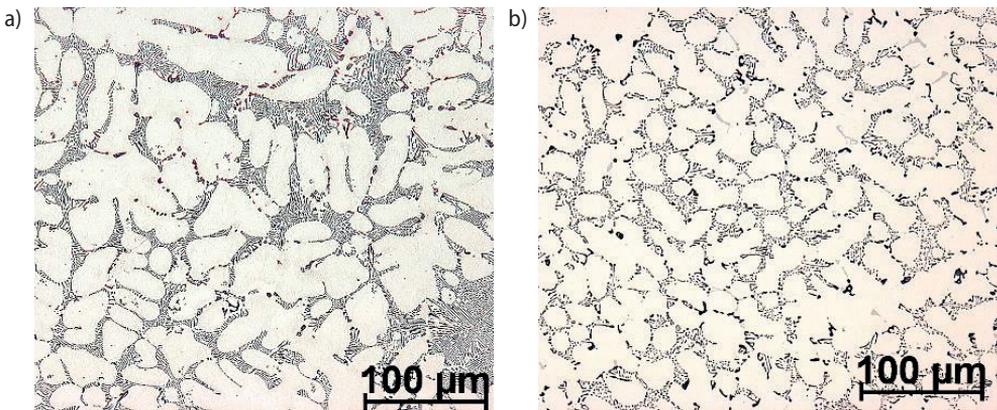

Fig. 4. Microstructure of specimens: as-cast microstructure of: a) specimen 1 cast into permanent mold; b) as-cast microstructure of specimen 2 subjected to HPDC

3.3. Element distribution in α-Al matrix

In spite of the morphological difference caused by the increased cooling rate for specimen 2, the element content for both specimens 1 and 2 varies only slightly. The Mg content in the solid solution of specimen 2 was about 1.30–1.40 wt.% (Fig. 5); whereas for specimen 1, it lies within the range of 1.25–1.42 wt.%. Examinations of Mg distribution across the grain in specimen 2 and dendrite arms in specimen 1 showed a lower Mg content in the area close to the center of grain or dendrite arm and its gradual increase in the direction towards the eutectic surrounding.
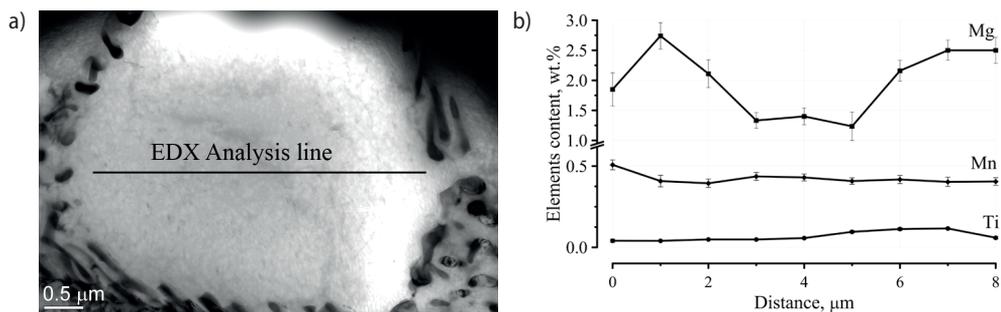
Fig. 5. Bright field image of separate grain in specimen 2 (a) and distribution of Mg, Mn and Ti across the grain (b)

For both specimens, the Mn content in the solid solution was about 0.3–0.4 wt.%, and no Mn-containing primary precipitates were observed. In the commercial alloy (specimen 2), a small Ti content was detected. Its distribution is inhomogeneous across α-Al grain, exhibiting a higher Ti content in the areas close to the centers and its gradual decrease to the near eutectic regions (Ti content of 0.07 wt.%). In some point, Ti contents reaching 0.33 wt.% were detected (Ti content up to 0.33 wt.%). The Si content in samples 1 and 2 were less than 0.1 wt.% or even smaller than the detection limit. EDX measurements performed on specimen 3 showed that the Si content in α-Al was about 0.9–1.2 wt.% and the Mg content 0.17–0.27 wt.%. The average composition of the α-Al matrix for all specimens is represented in Table 3.

Table 3. Average elements concentrations in α-Al solid solution measured for specimens 1–3

Specimen	Elements content, wt. %			
	Mg	Si	Mn	Al
1	2.20 ± 0.4	–	0.35 ± 0.05	98.65
2	2.00 ± 0.3	<0.1	0.41 ± 0.05	98.53
3	0.19 ± 0.03	0.91 ± 0.07	–	98.78

3.4. (Al) + (Mg$_2$Si) eutectic

Specimens 1 and 2 represent different morphologies of the (Al) + (Mg$_2$Si) eutectic. The eutectic in specimen 1 is mostly long-plate shaped, and the thickness of the Mg$_2$Si lamellas is about 1 μm, average interlamellae spacing is about 1.8 μm. The morphology of eutectic in specimen 1 after deep etching is represent in Figure 6a. In specimen 2, the eutectic is short and fibrous (Fig. 6b). Average lamella thickness is about 70–110 nm. The morphology of the (Al) + (Si) eutectic is represented in Figure 1a for non-modified condition.
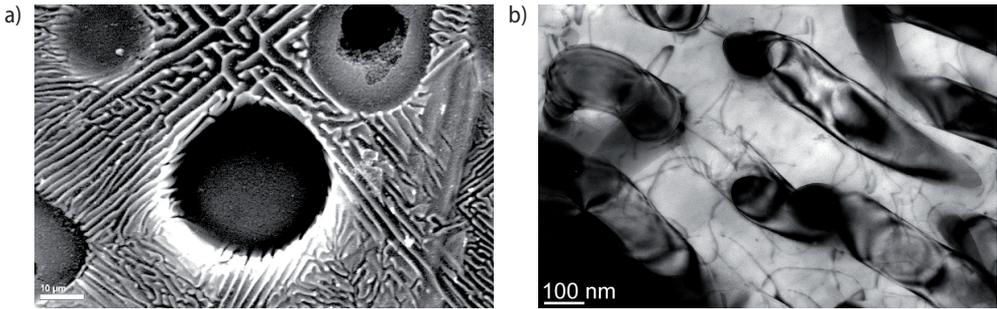
Fig. 6. (Al) + (Mg$_2$Si) eutectic morphology in specimen 1 (deep etching) (a) and bright field image of eutectic in specimen 2 (b)

3.5. Fe-containing phase

Inside the eutectic colonies in specimen 2, blocky particles were observed (Fig. 7). Their average size was about 2.0 μm. EDX measurements performed on 15 separate particles showed that this phase is enriched with Fe, Mn, and Si.

The average composition of this phase was (wt.%): 6.7–7.0 Fe, 18.0–23.0 Mn, 2.8–5.1 Si, 0.0–1.1 Mg, Al – the remainder. Measurements avoiding an overlap with matrix and eutectic material gave (wt.%): 4.8 Fe, 13.8 Mn and 3.3 Si. On this base, the Fe-containing phase can be identified as the α-Al$_{15}$(FeMn)$_3$Si phase.

For specimens 1 and 3 (prepared on a laboratory scale using pure Al and Mg), no Fe-containing phase was detected.

Fig. 7. Bright field image of Fe-containing phase in specimen 2

3.6. Precipitates

The most interesting results were obtained during TEM examinations of α-Al grains in specimens 1 and 2. The interior structure of solid solution grains is not homogeneous and contains randomly-distributed, curved, plate-like particles.

Detailed investigations of these precipitates revealed their features:
- composition of precipitates is very close to stoichiometric Mg_2Si compound,
- for both specimens 1 and 2, precipitates are aligned along dislocations,
- precipitation density is much higher for specimen 2 than for 1,
- precipitates are distributed only in the field of the solid solution, and precipitates were not detected between eutectic lamellas.

Experimental confirmation of these features is represented in Figure 8. The exact chemical composition of precipitates formed in specimens 1 or 2 cannot be measured due to the matrix contamination that appeared as a strong Al peak in the EDX spectrum. The effect of degradation of Mg-Si compounds was also observed.
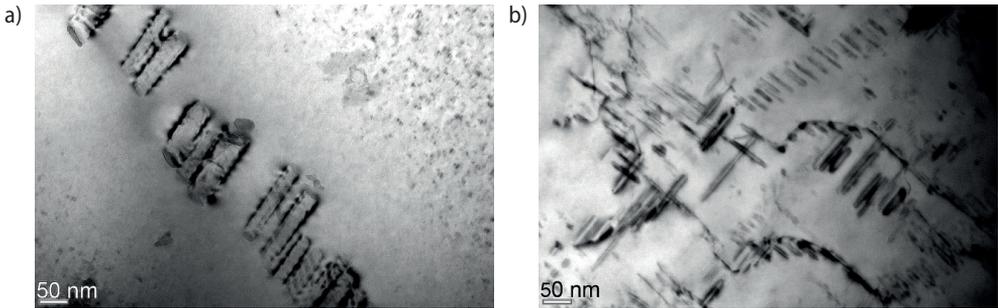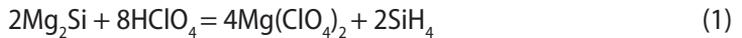
a)

b)

Fig. 8. Bright field image of precipitates observed in specimen: bright field image of precipitates in specimen 1 aligned along dislocation (a) and bright field image of precipitates in specimen 2 (b)

During electrolytic thinning of Al-Mg-Si alloys, the Mg-Si compound reacts with perchloric acid by the reaction (1):

$$2Mg_2Si + 8HClO_4 = 4Mg(ClO_4)_2 + 2SiH_4 \tag{1}$$

A small amount of O_2 can cause further oxidation of silane by the reaction (2):

$$SiH_4 + 2O_2 = SiO_2 + 2H_2O \tag{2}$$

As a result, Si is oxidized to form SiO_2 and Mg forms $Mg(ClO_4)$ that can dissolve in electrolyte. In this way, Mg-Si containing precipitates or eutectic lamellas in Al-Mg-Si alloys change their composition into a non-stichiometric compound.

A TEM examination of specimens 1 performed 3 hours after casting shows that there are no precipitate forms inside the Al matrix. The precipitates appear in samples examined after 3 days of exposure, or their growth were sometimes detected directly in the microscope column where thin foil affected by electron beam irradiation caused it to heat up to 200°C. From this observation together with the alignment of precipitates along dislocations, it can be concluded that the main mechanism of their formation is heterogeneous nucleation on dislocations during the natural aging of the alloys.

The high dislocation density in specimen 2 originated from differences in thermal expansion of α-Al and Mg$_2$Si together with pressure applied during HPDC, providing more nucleation sites for precipitates. Thus, precipitation density is much higher for specimen 2 than for specimen 1, and the presence of these precipitates resulted in high mechanical properties of AlMg5Si2Mn alloys in as-cast state. A confirmation of this was found after hardness measurements of specimen 1 and 2, where Brinell hardness of specimen 1 (HB = 71) was much lower than that of specimen 2 (HB = 96).

4. Discussion

Temperatures of endothermic processes detected in specimens 1, 2, and 3 are in good agreement with those identified from equilibrium Al-Mg-Si [13] and Al-Si [14] phase diagrams, subsequently. Recent DSC studies performed by Petkov et al. [9] gave an eutectic melting point for the commercial AlMg5Si2Mn alloy of 595,92°C and a peak temperature of 607.1°C, which is in good agreement with temperatures detected by our DSC measurements of samples 1 and 2.

Age hardening of Al-Si-Mg alloys is known to be a sequence of precipitations, namely GP-zone formation, β'' and/or β' transitional phases. The exothermic peak at 220–260°C found in specimen 3 DSC plots corresponds to the precipitation of coherent β'' phase that is in agreement with observations of Wang et al. [12]. Such a precipitation can take place in an alloy at slightly elevated temperatures or even in an as-cast condition; i.e., without preliminary solution treatment and quenching.

Comparing the heating behavior of specimens 1 and 2, it can be concluded that the thermal history of the sample does not play an essential role in the reaction temperatures. However, for both samples, there was no low temperature effect as in specimen 3 (see Fig. 3c). This can be related to the different composition of the solid solution of the samples investigated (Tab. 3). The α-Al matrix of specimen 3 contains 0.19 wt.% Mg and 0.91 wt.% Si, which is enough to supply a density of β'' phase, which is high enough to be detected by DSC. In contrast, even for HPDC specimen 2, the average Mg content in the solid solution is about 2.1 wt.%, but the Si concentration is below 0.1 wt.%. Thus, the precipitate density for specimens 1 and 2 will be much lower and the heat effect below the limit of detection.

TEM observations clearly show that plate-like precipitates are present in specimens 1 and 2 in as-cast conditions. These particles are found in the α-Al grains in the center and close to the eutectic as well. They form without any heat treatment. From their alignment along dislocations, it is most likely that they form via heterogeneous nucleation and that dislocations provide nucleation sites for their growth. Heterogeneous nucleation of precipitates in Al-Mg$_2$Si alloys on dislocations is a well-established mechanism during the decomposition of a solid solution. However, in most cases, this effect was considered for wrought alloys undergoing artificial aging. For casting alloys in cast condition, however, the direct formation of such a type of precipitates was not yet established.
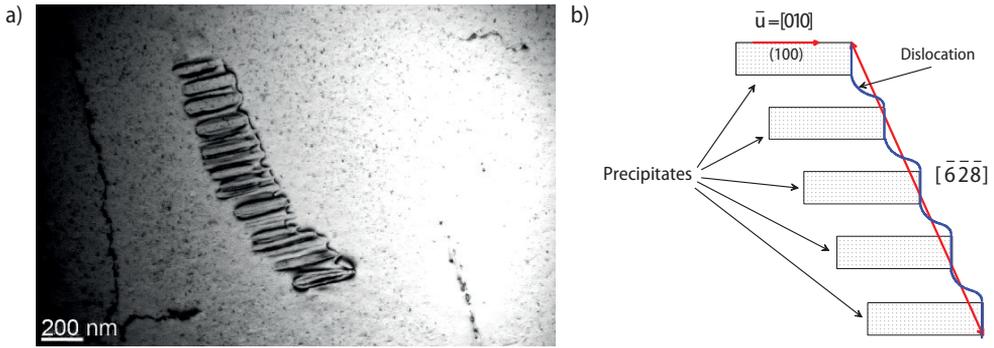
Fig. 9. Enlarged view of precipitates in specimen 1: a) dislocation marked by arrows; b) schematic presentation of precipitates and dislocation

An enlarged view of the precipitates in specimen 1 is shown in Figure 9a. The schematic presentation of the zebra-crossing structure is given in Figure 9b. Tilting the specimen to different zone axes and using different reflections for diffraction contrast allowed for reconstruction of the geometry of this structure and the nature of the dislocation. The plates lie in (100) planes, their long axis is [010]. The dislocation has Burgers vector $\bar{b} = \pm \frac{1}{2}[10\bar{1}]$. It connects the plates on the right side in a curved line that can be described by the average direction $[\bar{6}\,\bar{2}\,8]$ or simplified [101]. So the plates do not lie in one (100) – plane, but are shifted in [100] and [001] direction. The dislocation forms a loop around each precipitate. Along the long side of the precipitate, the dislocation segment has line vector [010] and Burgers vector, $\bar{b} = \pm \frac{1}{2}[10\bar{1}]$ i.e., this is an edge dislocation.

The observation that high dislocation density is connected with a high density of precipitates supports our presumption that the nucleation of precipitates takes place on dislocations. In specimen 2, the density of dislocations is much higher, and the precipitation density is larger than that for specimen 1. Probably the reason for the dislocations is thermal stresses between α-Al and Mg_2Si intermetallics and extrusion stresses during the HPDC process. When no pressure was applied during mould filling and solidification (specimen 1), the precipitate density is much lower. So obviously, pressure plays a more important role for dislocation generation than thermal stress.

Ravi and Wolverton [15] found that, for Mg-rich alloys, the formation of Mg_5Si_6 is energetically more favorable than other possible precipitates. In our alloys, we found that areas with precipitates show enrichment with Mg and Si. So, it is most likely that these precipitates are β'' phase.

The strengthening role of precipitates formed via natural aging can be simply verified by the results of hardness and microhardness measurements. The highest hardness HB = 95 and microhardness $HV_{0.05} = 96$ kgf·mm^{-2} were measured for specimen 2, where precipitation density is much higher than for specimen 1. The lowest hardness HB = 73

and $HV_{0.05}$ = 69 kgf·mm^{-2} were found for specimen 1, where the precipitate density is lower than in specimen 2.

Similar precipitates were observed in the as-caste condition of different casting alloys. Precipitates formed after one-week natural aging in the (Al-Cu) casting alloy A201 cast into a permanent mould. Additional research showed similar precipitation behavior of the Al-Mg-Si-Mn casting alloys after additional alloying with Sc + Zr, Li, Ti + Zr. This could be a starting point for the development of Li-containing casting alloys, where density is decreased and strength is improved simultaneously by precipitation hardening.

5. Conclusions

The results of the study of melting behavior, microstructure, and precipitation in the AlMg5Si2Mn alloy can be summarized as follows:

1. Both samples of the AlMg5Si2Mn alloy produced via the PM and HPDC routes show similar behavior on heating. The eutectic melting temperature was found at 596.2°C – about 20°C higher than that of the PM A356 alloy. The latter shows an exothermic effect at low temperature part of DSC trace, thus confirming that the decomposition of the solid solution may start directly from the as-cast state. This low temperature precipitation reaction was not observed for the AlMg5Si2Mn alloy.

2. Phase morphologies are different for the PM and HPDC AlMg5Si2Mn alloys. In the PM casting alloy where the cooling rate is about 2 K·s^{-1}, α-Al grains are dendritic with well-developed branches, whereas the HPDC alloy (cooling rate of 60 K·s^{-1}) exhibits rosette-like grains with the size one order of magnitude lower than the PM alloy.

3. Properties of the HPDC AlMg5Si2Mn alloy are related to the precipitation of plate-like precipitates, which is heterogeneously nucleated on dislocations. These precipitates are most obvious β'' phase randomly distributed inside solid solution grains. The density of precipitates is related to the density of dislocations. Larger precipitation density was found in the HPDC alloy and are formed due to applied pressure on metal during solidification.

References

[1] Pacz A.: US Patent No. 1,387,900: Aluminum-Silicon Alloy. Patented August 16, 1921

[2] Pacz A.: US Patent No. 2,013,926: Modification of aluminum, aluminum alloys and alloys containing aluminum. Patented September 10, 1935

[3] Wilm A.: Physikalisch – metallurgische Untersuchungen über magnesiumhaltige Aluminiumlegierungen, Metallurgie, 8 (1911), 225–227

[4] Duparc O.H.: Alfred Wilm and the beginnings of Duralumin. Zeitschrift für Metallkunde, 96, 4 (2005), 398–404

[5] Wang Q.G. and Davidson C.J.: Solidification and precipitation behaviour of Al-Si-Mg casting alloys. Journal of Materials Science, 36 (2001), 739–750

[6] Apelian D., Shivkumar S., and Sigworth G.: Fundamental Aspects of Heat Treatment of Cast Al-Si-Mg Alloys. AFS Transactions, 97 (1989), 727–742

[7] Wuth M.C., Koch H., Franke A.J.: Production of steering wheel frames with an AlMg5Si2Mn alloy. Casting Plant and Technology International, 16, 1 (2000), 12–24

[8] Otarwanna S., Gourlay C.M., Laukli H.I., and Dahle A.K.: Microstructure Formation in AlSi4MgMn and AlMg5Si2Mn High-Pressure Die Castings. Metallurgical and Materials Transactions A, 40, 7 (2009), 1645–1659

[9] Petkov T., Kunstner D., Pabel T., Faerber K., Kneissl C. und Schumacher P.: Erweiterung des Eigenschaftspotentials der Legierung AlMg5Si2Mn durch eine gezielte Wärmebehandlung Berg- und Hüttenmännische Monatshefte, X (2013), 1-9, Jvn. Jg. (2013), Heft X© Springer-Verlag Wien, 1–9

[10] Miao W.F., Laughlin D.E.: A differential scanning calorimetry study of aluminum alloy 6111 with different pre-aging treatments. Journal of Materials Science Letters, 19 (2000), 201–203

[11] Vedani M., Angella G., Bassani P., Ripamonti D., and Tuissi A.: DSC analysis of strengthening precipitates in ultrafine Al-Mg-Si alloys. Journal of Thermal Analysis and Calorimetry, 87, 1 (2007), 277–284

[12] Wang G., Yan L., Ren G., and Zhao Z.: Analyzing As-Cast Age Hardening of 356 Cast Alloy. Journal of Materials Engineering and Performance, 20, 4 (2011), 399–404

[13] Barabash O.M., Sulzhenko O.V., Legkaya T.N., and Korzhova N.P.: Experimental analysis and thermodynamic calculation of the structural regularities in the fusion diagram of the system of alloys Al-Mg-Si. Journal of Phase Equilibria, 22, 1 (2001), 5–11

[14] Vander Voort G.F. and Asensio-Lozano J.: The Al-Si Phase Diagram. Microscopy and Microanalysis, 15, Supplement S2 (2009), 60–61

[15] Ravi C., Wolverton C.: First-principles study of crystal structure and stability of Al-Mg-Si-(Cu) precipitates. Acta Materialia, 52 (2004), 4213–4227